A Low-Frequency Versatile Wireless Power Transfer Technology for Biomedical Implants

Hao Jiang, *Member, IEEE*, Junmin Zhang, Di Lan, *Student Member, IEEE*, Kelvin K. Chao, Shyshenq Liou, *Member, IEEE*, Hamid Shahnasser, *Member, IEEE*, Richard Fechter, Shinjiro Hirose, Michael Harrison, and Shuvo Roy, *Member, IEEE*

***Abstract*—Implantable biomedical sensors and actuators are highly desired in modern medicine. In many cases, the implant's electrical power source profoundly determines its overall size and performance [1]. The inductively coupled coil pair operating at the radio-frequency (RF) has been the primary method for wirelessly delivering electrical power to implants for the last three decades [2]. Recent designs significantly improve the power delivery efficiency by optimizing the operating frequency, coil size and coil distance [3]. However, RF radiation hazard and tissue absorption are the concerns in the RF wireless power transfer technology (RF-WPTT) [4], [5]. Also, it requires an accurate impedance matching network that is sensitive to operating environments between the receiving coil and the load for efficient power delivery [6]. In this paper, a novel low-frequency (< 1 kHz) wireless power transfer technology (LF-WPTT) using rotating rare-earth permanent magnets is demonstrated. The LF-WPTT is able to deliver 2.967 W power at ~ 180 Hz to an 117.1 Ω resistor over 1 cm distance with 50% overall efficiency. Because of the low operating frequency, RF radiation hazard and tissue absorption are largely avoided, and the power delivery efficiency from the receiving coil to the load is independent of the operating environment. Also, there is little power loss observed in the LF-WPTT when the receiving coil is enclosed by non-magnetic implant-grade stainless steel.**

***Index Terms*—Biomedical implants, inductive coupling, wireless power transfer.**

I. Introduction

BIOMEDICAL implants have been widely used in various applications ranging from traditional cardiac pacemakers [7] to emerging retina prostheses [8], brain computer interfaces [9], drug delivery [10] and smart orthopedic implants [11]. Even after decades, delivering electrical power to implants is still the most critical challenge to their function and performance, which include size, life-span, signal processing capability of electronics, and data rate of wireless telemetry [1]. Non-rechargeable batteries can only support implants with extremely low power consumption. For example, the battery of a pacemaker, whose power consumption is about 8 μW [7], occupies 90% of the total device volume [12]. In addition, it must be replaced by costly invasive surgery every 5–8 years [13]. Other implants, such as the interventional orthopedic implants [11] and the mechanical pump based cardio implants [14], require high power, to operate, and therefore cannot be powered by a non-rechargeable battery. Although life-saving, implant technology is severely restricted by the battery size, the available power, and the costs associated with its limited life-span. Thus, there is an immanent need for a wireless power transfer technology (WPTT) that is capable of delivering significant amounts of electrical power to implants in a safe and noninvasive manner.

The air-core based radio-frequency wireless power transfer technology (RF-WPTT) with two face-to-face inductive coils has been the primary approach to wirelessly power implants [2]. Although energy harvesting from bio-surroundings using nanotechnology is a much more elegant solution, the scavenged power is still in the nW range that is not powerful enough to drive most implants [15]. The WPTT using ultrasound has the advantage of penetrating bio-tissues with minimal loss. However, the delivered power and efficiency is quite limited at this stage [16]. So far, the RF-WPTT has been widely studied and adopted for various biomedical implants [17].

The RF-WPTT could pose some challenges in clinical applications when operating at high-frequencies. To pursue high power delivery efficiency and a smaller receiving coil size, the operating frequency of the RF-WPTT has been increased to the GHz range [18]–[20]. At this frequency, accurate impedance matching is needed in both the transmitting and receiving circuits to achieve the desired power delivery efficiency [8]. Moreover, the impedances of the both transmitting and receiving coils are uncertain in many clinical applications, because they are sensitive to the distance and the orientation between the transmitting and the receiving coil [21], as well as the electrical properties of the bio-tissues between the coils [22]. The requirements of the meticulous alignment between the coils and the accurate knowledge of the electrical properties of the transmission medium could be a challenge in clinical applications. Also, conductive bio-tissues could significantly reduce the delivered power in the RF range due to absorption [23].

Inspired by the wirelessly-driven magnetic gear that is used to deliver mechanical power from an *ex-vivo* rotor to an *in-vivo* rotor [24], a novel low-frequency wireless electrical power

Manuscript received February 23, 2012; revised May 19, 2012; accepted September 03, 2012. Date of publication December 25, 2012; date of current version July 24, 2013. This work was supported in part by Linear Technology Corporation and the Pediatric Device Consortium at the University of California, San Francisco, an FDA Grant Program (Award 5P50FD003793-02). This paper was recommended by Associate Editor M. Ghovanloo.

H. Jiang, J. Zhang, D. Lan, K. K. Chao, S. Liou, and H. Shahnasser are with the School of Engineering, San Francisco State University, San Francisco, CA 94132 USA (e-mail: jianghao@sfsu.edu).

R. Fechter, S. Hirose, and M. Harrison are with Department of Surgery, University of California, San Francisco, San Francisco, CA 94143 USA.

S. Roy is with Department of Bioengineering and Therapeutic Sciences, University of California, San Francisco, San Francisco, CA 94107 USA.

Color versions of one or more of the figures in this paper are available online at http://ieeexplore.ieee.org.

Digital Object Identifier 10.1109/TBCAS.2012.2220763

transfer technology (LF-WPTT) that operates around hundreds Hz is presented in this paper. Such a low operating frequency changes the paradigm of the WPTT's design. In order to harvest enough power at such a low operating frequency, a strong magnetic field is needed. Because a magnetic field generated by rare-earth permanent magnets is far stronger than that produced by a simple electronic system, rotating rare-earth permanent magnets are used to deliver the same amount of electrical power to an inductive coil at a much lower frequency [25].

Several advantages are derived from this low-frequency operation: At < 1 kHz frequency range, the RF radiation hazard is completely avoided [4]. The resistance instead of the reactance dominates the impedance of the receiving coil because of the low operating frequency. The former is unlikely to change depending on the application. Thus, the impedance matching for the efficient power transfer from the receiving coil to the load does not tie in with various operating conditions. Because of the low operating frequency, various ferrite materials can be used in the receiving coil to enhance the coupling without worrying about their hysteresis response time [26]. Moreover, a slow-varying magnetic field from rotating permanent magnets is able to penetrate various non-magnetic materials, including conductive bio-tissues and implant-grade stainless steel housing without significant loss.

In this paper, the LF-WPTT is described in Section II. Its delivered power and efficiency are measured and analyzed in Section III. In Section IV, the versatility of the LF-WPTT is demonstrated experimentally. The advantages and disadvantages of the LF-WPTT are discussed in Section V, followed by the conclusions.

II. The Method

In the LF-WPTT, the time-varying magnetic field is generated by rotating permanent magnets and captured by a stationary inductive receiving coil. The electrical power is induced in the receiving coil by the time-varying magnetic field, like an electrical generator.

A. The Strong Magnetic Flux Produced by Permanent Magnets

To compensate the low-frequency operation, strong magnetic field produced by permanent magnets is employed in the LF-WPTT. The magnet used here is made of neodymium iron boron (NdFeB) [27], which is one of the strongest permanent magnets. A finite-element multi-physics simulation package, COMSOL [28], is employed to determine how much electrical current would be needed in a single-turn coil to generate the equivalent magnetic flux produced by the permanent magnet. In this simulation, the magnetization of the magnet is set to be 75,000 A/m as suggested in the magnets data sheet [27]. For a disk magnet with 19 mm (3/4 inch) in diameter and 3 mm (1/8 inch) in thickness, the magnetic flux density distribution on the disks outer surface is plotted as the solid line in Fig. 1. The total magnetic flux on the disk magnets surface is estimated as ~ 63 μWb from the simulation. To achieve the same amount of the magnetic flux in a single-turn current loop with the same diameter, the needed current is about 3.5 kA. The magnetic flux density distribution of a single-turn current loop is plotted as the dashed line in Fig. 1. In this paper, rotating permanent magnets driven by an electrical DC motor, instead of an inductive coil driven by a high-current low-frequency electronics, are used to generate the high-strength low-frequency magnetic flux.

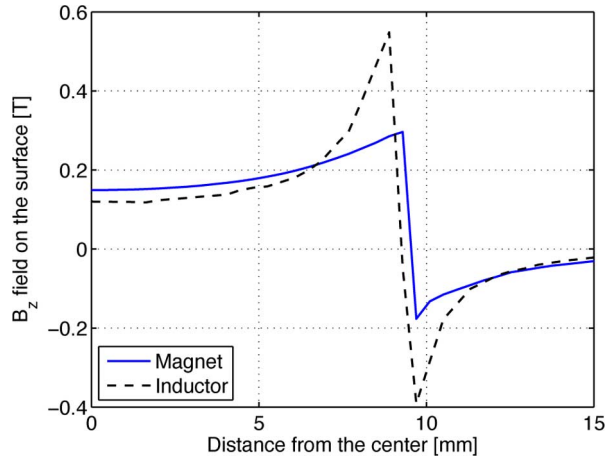

Fig. 1. The radial distribution of the vertical (i.e., normal to the disk or the loop) magnetic flux density B_Z on the surface of (a) a disk magnet (solid line) and (b) a single-turn current loop (dashed line).

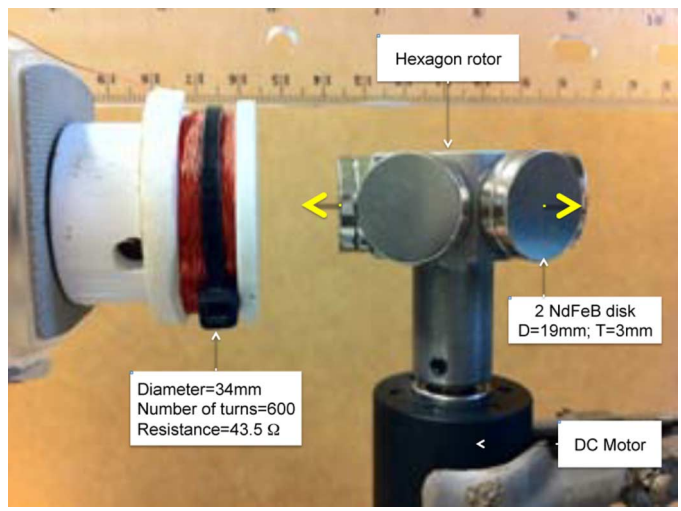

Fig. 2. This is a picture of the rotary system with magnets and the receiving coil. All the arrows on the disk magnets point to North. The receiving coil is a hand-wound, 600-turn solenoid with the diameter of 34 mm.

B. The Rotating Permanent Magnets

The setup of the LF-WPTT used in this paper is shown in Fig. 2. There are two disk magnets attached to the each side of an iron hexagon rotor.[1] Each NdFeB disk magnet is 19 mm (3/4 inch) in diameter and 3 mm (1/8 inch) in thickness. The magnetization direction of these disk magnets is perpendicular to their circular surface. Neighboring magnets are arranged to have opposite polarity pointing the magnetic north pole in or out to achieve maximum magnetic field variation in the coil. The thickness of the rotor is also 19 mm and the diameter of the hexagon rotor is 38 mm so that the edge surface of this rotor is a 19×19 mm square. The iron hexagon rotor is connected to an

[1]It is not necessary for the rotor to be hexagonal. Other polygonal rotors with an even number of sides may also be used. Adjacent magnets need to have opposite polarity to achieve maximum power delivery.

Fig. 3. The picture of the DC motor and the receiving coil used in this paper. The motor is from Faulhaber (Model: 3272G012CR). The coil is hand-wound with 600 turns and a diameter of 34 mm. The wire diameter is 0.025 mm.

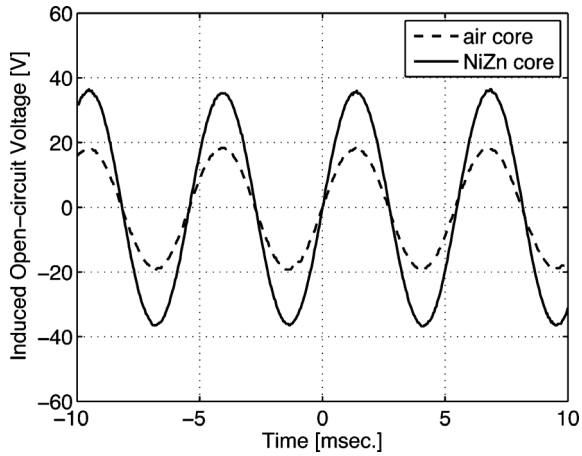

Fig. 4. The induced open-circuit voltage versus time from the receiving coil with the air core and the ferrite core at a distance (i.e., from the disk magnet to the receiving coil) of 10 mm.

electric DC motor via a machined shaft. The DC motor used here is about 7-cm in length and 2.5-cm in diameter [29], as shown in Fig. 3. Because the rotor is made of regular iron, the disk magnets can be attached to the hexagonal rotor by the magnetic attraction force and rotated together. In this way, the rotation of disk magnets can be achieved without machining the magnets themselves. Thus, the time-varying magnetic flux is produced by the rotation of the hexagon rotor.

C. The Receiving Coil

Based on Faraday's Law, the induced open-circuit voltage v_{OC} of the receiving coil in the LF-WPTT is

$$v_{OC} = N\frac{d\psi(D,d)}{dt}. \tag{1}$$

Here, N is the number of turns of the receiving coil, and $\psi(D,d)$ is the magnetic flux captured by the coil. The captured magnetic flux $\psi(D,d)$ is a function of both the diameter of the receiving coil D and the distance between the coil and the magnet d (they are illustrated in Fig. 10). When the diameter of the coil is less than that of the disk magnet, some ψ from the magnet will not be captured. If the diameter of the coil is much larger than that of the disk magnet, the overall captured ψ will also be reduced because the flux produced by the adjacent magnet has the opposite direction. The diameter of the receiving coil used here is 34 mm. The coil has 600 turns and about 10 mm in length, as shown in Fig. 3. With a bundle of ferritic NiZn rods [30] with 5 mm diameter in the core, the coil's inductance and resistance are and 34 mH and 43.5 Ω, respectively. This coil is used throughout this paper unless otherwise specified.

D. The Induced Open-Circuit Voltage v_{OC}

The induced open-circuit voltage v_{OC} can be accurately measured by connecting the receiving coil's two-ends to an oscilloscope's high-impedance probe directly. The waveforms of the induced open-circuit voltage with and without a ferrite core are captured in Fig. 4. The distance between the coil and the disk magnet d is 10 mm and the rotor rotates at ∼60 revolutions per second. In Fig. 4, the waveform of the coil with a ferrite core is sinusoidal and reaches 36.4 V at ∼ 180 Hz (3× of the motor's rotating frequency when a hexagonal rotor is used).

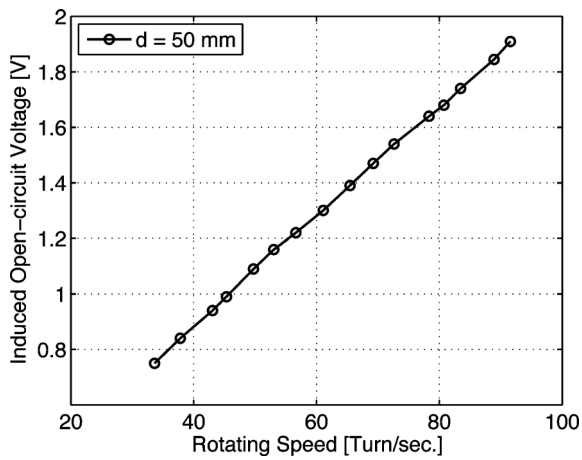

Fig. 5. The induced open-circuit voltage versus the motor's rotating speed at the distance of 50 mm.

E. v_{OC} at Different Rotating Speeds

One way to control v_{OC} is to change the rotors rotating speed, as indicated in (1). The rotating speed of the DC motor can be controlled by its supply voltage [29]. v_{OC} is measured at different motors rotating speeds, when the receiving coil is placed 50 mm away from the rotating magnets. The measurement results are plotted in Fig. 5. The linear relationship depicted in Fig. 5 is consistent with the above analysis and provides a possible approach to control the delivered power in the LF-WPTT.

III. The Delivered Power and Efficiency

In this section, the delivered power and the efficiency of the LF-WPTT are analyzed, measured and discussed. Following [31], the power flow and various power losses in the LF-WPTT are illustrated in Fig. 6. First, power from the external source, P_E, is consumed to rotate the magnets. Ideally, no power is needed for rotating a rotor at a constant speed alone (without the receiving coil) due to the rotation inertia. However, in reality, there is a power loss to overcome the rotors own loss. Once the receiving coil is engaged (close to the rotating magnets), the rotor requires extra power, P_T, to overcome the drag force caused by the induced current in the receiving coil. The

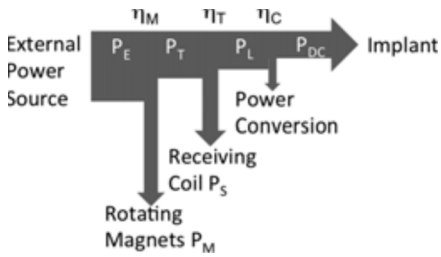

Fig. 6. The power flow diagram in the LF-WPTT.

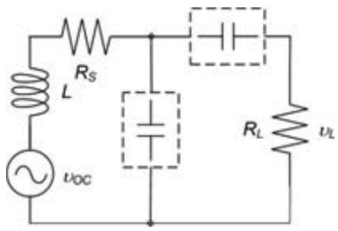

Fig. 7. An equivalent circuit of the receiver. v_{OC} is the induced open-circuit voltage from the receiving coil. L and R_S are the inductance and resistance of the receiving coil. R_L is the load resistor. v_L is the voltage across the load resistor.

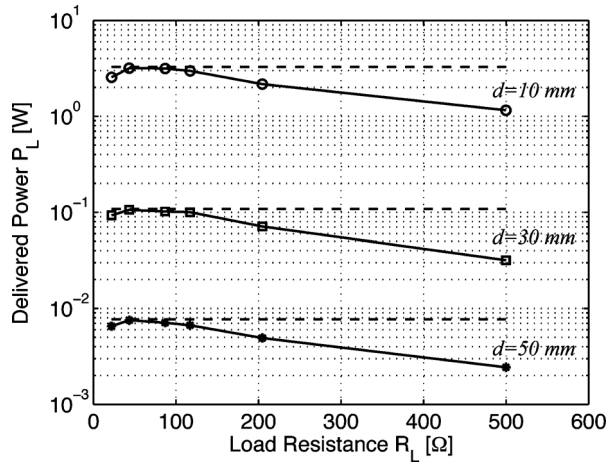

Fig. 8. The delivered power P_L (estimated via the measured voltage across the load resistor v_L) is plotted versus different load resistance at the distance of 10 mm (the solid line with circles), 30 mm (the solid line with squares) and 50 mm (the solid line with asterisks). The maximum deliverable power, $P_{L,\max}$, (estimated via the measured open-circuit voltage v_{OC}) is also plotted as the dashed lines.

power induced in the receiving coil is split between the power delivered to the rest of the load, P_L, and the power dissipated by the receiving coil, P_S. In this section, the discussion focuses on P_L and the overall power transfer efficiency, η_{OV}, which is the ratio of the delivered power to the load, P_L, to the total power consumed by the electric motor, P_E.

A. The Delivered Power

The delivered power is important for most of implants [1]. An equivalent circuit, depicted in Fig. 7, is used to analyze the delivered power to a load in the LF-WPTT. Similar to the far-field RF-WPTT described in [32], the impedance of the receiving coils is independent of the mechanical-electrical coupling. The v_{OC} represents the induced open-circuit voltage. L and R_S are the inductance and parasitic series resistance of the receiving coil, respectively. R_L is the load resistor. In contrast to the RF-WPTT, the matching capacitor in the dashed line box is purposely neglected here because of the low frequency. The voltage developed across the load resistor, v_L, can be calculated as

$$v_L = v_{OC}\frac{R_L}{j\omega L + R_S + R_L}. \tag{2}$$

Thus, the delivered power, P_L, can be calculated as

$$P_L = \frac{1}{2}\frac{v_L^2}{R_L}. \tag{3}$$

In the RF-WPTT, ωL in (2) is significantly larger than R_S and R_L, therefore, a matching capacitor, either in-parallel or in-series with R_L (shown as the dashed line boxes in Fig. 7), is needed to achieve the conjugate match between the receiving coil and the load resistor for the maximum power transfer [33], if desired. Because the impedance of the coil correlates to the coupling with the transmitting coil [34], as well as the dielectric properties of its surroundings [22], choosing the right value of the matching capacitor for various operating conditions is often challenging.

Because the LF-WPTT is able to operate at low frequencies due to the superior strength of the magnetic field produced by the rare-earth permanent magnets, the impedance matching for the maximum power delivery is drastically different compared to that of the RF-WPTT. At low frequencies, ωL is negligible compared to R_S and R_L, therefore, (2) can be simplified to

$$v_L \approx v_{OC}\frac{R_L}{R_S + R_L}. \tag{4}$$

When R_L is close to R_S, the delivered power P_L is

$$P_L \approx \frac{1}{8}\frac{v_{OC}^2}{R_S}. \tag{5}$$

In theory, if there is a perfect conjugate match between the receiving coil and the load resistor, the maximum deliverable power to the load is [35]

$$P_{L,\max} = \frac{1}{8}\frac{v_{OC}^2}{R_S}. \tag{6}$$

Thus, as shown in (5) and (6), once the load resistance and the receiving coil's resistance are matched, the delivered power is close to the maximum in the LF-WPTT without matching capacitors.

In the experiment, the delivered power is obtained based on the measured voltage across a load resistor that is directly connected to the receiving coil. In low frequencies, a regular oscilloscope with a high-impedance probe can accurately measure the voltage across the load resistor. The delivered power, P_L, thus can be obtained via (3). The same coil with 43.5 Ω series resistance is used in this experiment. The delivered power at different load resistances is summarized in Fig. 8 when the receiving coil is placed at 10 mm away from the rotating magnets. The maximum deliverable power estimated via (6) based on the measured open-circuit voltage is also included in Fig. 8 as the dashed lines.

The measurement results in Fig. 8 indicate that the delivered power, P_L, is very close to $P_{L,\max}$ when R_L matches with R_S without any matching capacitors, as predicted by the above analysis. When d is 10 mm, the maximum delivered power on a 43.5 Ω load resistor is 3.170 W, and the maximum deliverable power estimated based on the open-circuit voltage v_{OC} via (6) is 3.225 W. Without any matching capacitors, P_L is able to reach 98% of $P_{L,\max}$. Also, the measurement results in Fig. 8 show that the delivered power is not dramatically reduced when the load resistance is off from the optimal value. When d is 10 mm, P_L only drops 1% (3.154 W) and 6% (2.976 mW) when the load resistance is $\sim 2 \times (86.8\ \Omega)$ and $\sim 3 \times (117.1\ \Omega)$ of the optimal value ($R_L = R_S = 43.5\ \Omega$), respectively. Furthermore, the measurement results show that the maximum power delivery is achieved under the same matching condition ($R_L = 43.5\ \Omega$) when the receiving coil is placed at different distances, from 10 mm to 50 mm.

B. The Efficiency

When the *ex-vivo* power source is required to be mobile or wearable, the efficiency of the wireless power transfer technology becomes critical. In this paper, the overall power transfer efficiency, η_{OV} is characterized by the ratio of the delivered AC power to a resistive load, P_L, to the total power consumed by the DC motor, P_E. There is also some power loss associated with converting the induced AC power to the steady-state DC power. Since the power conditioning circuit is outside the scope of this paper, it is not considered here.

In the experiment, a constant DC voltage, $V_E = 8.5$ V, is applied to the DC motor [29] to achieve a constant rotation speed (~ 60 rotation/sec.). Its supply current, I_E, is used to monitor the motors power consumption. When the receiving coil is far away from the rotating magnets, the power consumed by the DC motor, $P_{E,0}$, is 1.445 W ($I_{E,0} = 0.170$ A). Once the receiving coil is close to the rotating magnets, the DC motor needs to consume more current, I_E, to maintain its constant rotation speed. The extra power consumed by the motor, P_T, which is largely due to the magnetic field produced by the induced current in the receiving coil, can be estimated from the increase of I_E as $V_{DC}(I_E - I_{E,0})$. P_L is calculated based on the measured voltage across the load resistor that is directly connected to the receiving coil via (3), as depicted in Fig. 7.

The power and the associated efficiency are measured and summarized in Table I, when R_L is close to R_S and $3 \times R_S$. In the LF-WPTT, the load resistance for the maximum output power is different from the maximum power efficiency, similar to the two-coils RF-WPTT [33]. Table I shows that the overall power transfer efficiency η_{OV} reaches 50% with 2.967 W output power when the load resistance is about $3\times$ of the receiving coil's parasitic series resistance R_S. When the load resistance is the same as R_S, η_{OV} drops to 33.6% even though the output power is increased to 3.170 W. In the experiment, the receiving coil is 10 mm away from the rotating magnets.

To further investigate R_L's impact on η_{OV}, the power and its associated efficiency are measured and plotted with various load resistances, as depicted in Fig. 9. The measured P_L peaks when R_L is 43.5 Ω and equals to R_S. At this point, because R_L and R_S are in series, both P_L and P_S reach the maxima. When

TABLE I
THE POWER AND THE EFFICIENCY ASSOCIATED WITH THE LF-WPTT AT A DISTANCE OF 10 MM

$I_{E,0}$= 0.170 [A]	R_L=43.5 [Ω]	R_L=117.1 [Ω]
I_E [A]	1.110	0.700
P_E [W]	9.435	5.950
P_T [W]	7.990	4.505
v_L [V]	16.60	26.4
P_L [W]	3.170	2.967
η_{OV} [%]	33.6	50.0

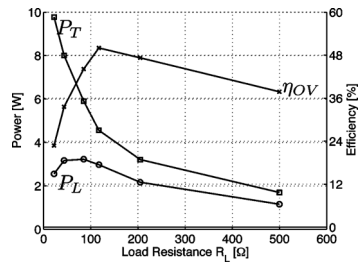

Fig. 9. The measured power delivered to the load resistor, P_L, and the extra power needed for driving the motor at the constant rotating speed, P_T, are plotted versus the load resistance, R_L, as the solid line with circles and the solid line with squares, respectively. The overall power transfer efficiency, η_{OV}, is plotted as the solid line with crosses.

R_L increases from 20 Ω to 500 Ω, the extra power needed for driving the motor at the constant rotating speed, P_T, (the solid line with square in Fig. 9) reduces dramatically, as depicted in Fig. 9. As depicted in Fig. 7, the increase of R_L reduces the current in the receiving coil, thus, less P_T is needed. Because of the dramatic reduction of P_T, and consequently P_E, η_{OV} (the solid line with crosses in Fig. 9) peaks with 50% when R_L is 117.1 Ω.

IV. VERSATILITY

The versatility of the LF-WPTT is demonstrated in this section. The performance of the technology is characterized with various operating distances, geometrical misalignments, and operating environments, including placement of the receiving coil in the saline (to emulate the conductive bio-tissues) and non-magnetic implant-grade stainless steel housing.

A. The Distance

In the LF-WPTT, the power delivery efficiency from the receiving coil to the load remains the same at various distances, as described in the previous section. The power delivered to the load is only subject to the magnetic coupling between the rotating magnets and the receiving coil.

In the experiment, the voltage across the load resistor, v_L, is measured as a function of the distance d, which is defined as the distance from the surface of the disk magnet to the top surface of the receiving coil, as shown in Fig. 10. The receiving coil is directly connected to a load resistor. At each distance d, v_L is measured at two different load resistance, 43.5 Ω (for the maximum P_L) and 117.1 Ω (for the maximum η_{OV}). The corresponding delivered power is calculated using (3) and plotted in Fig. 11.

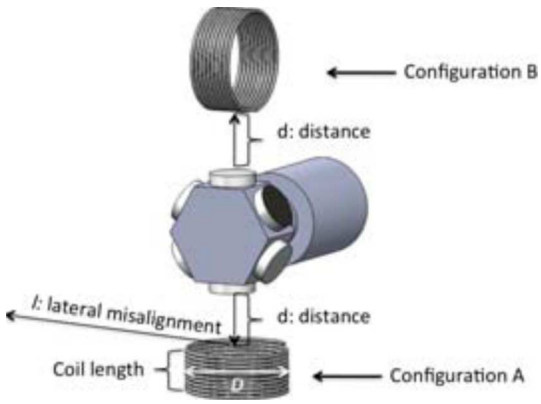

Fig. 10. An illustration of the experimental setup. The hexagonal rotor is driven by an electrical DC motor. The disk magnets are attached to the iron hexagonal rotor by magnetic attraction forces. D is the diameter of the receiving coil. d is the distance from the disk magnet to the receiving coil. In the lateral misalignment measurement, the coil moves horizontally as indicated in arrow labeled as "l: lateral misalignment". In the angular misalignment measurement, the coil is placed as the Configuration A or B.

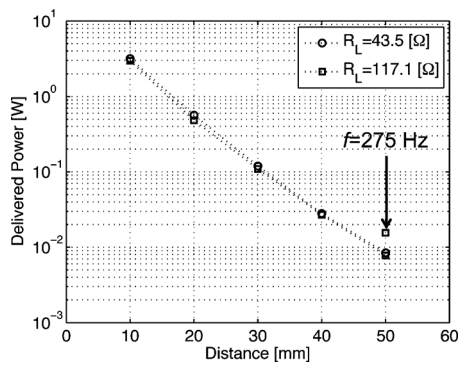

Fig. 11. The delivered power at 180 Hz is calculated based on measured v_L via (3) and plotted versus distance d when the load resistance is 43.5 Ω (shown as the dotted line with circles) and 117.1 Ω (shown as the dotted line with squares). At 50 mm, the delivered power to a 117.1 Ω resistor at 275 Hz is shown as the square.

The measurement results in Fig. 11 show that the maximum delivered power ($R_L = 43.5\ \Omega$) reaches 3.17 W and 8.4 mW over 10 mm and 50 mm distance, respectively. When the maximum overall efficiency is achieved ($R_L = 117.1\ \Omega$), the delivered power reaches 2.98 W and 7.8 mW over 10 mm and 50 mm distance, respectively. Because the magnets rotating speed is maintained at 60 revolution per second, the power loss over the distance is largely due to the magnetic field fading when the receiving coil is moved away from the magnets.

When the coil is away from the magnets, the delivered power can be increased by increasing the motor's supplying voltage, and consequently, the magnets' rotating speed. When the coil moves from 10 mm to 50 mm away from the magnets, the motor's supplying current reduces from 700 mA to 180 mA at 8.5 V supplying voltage to maintain 60 revolution per second. When the supply voltage is increased to 12.5 V, the delivered power to a 117.1 Ω resistor is increased from 7.8 mW (at 180 Hz) to15.6 mW (at 275 Hz).

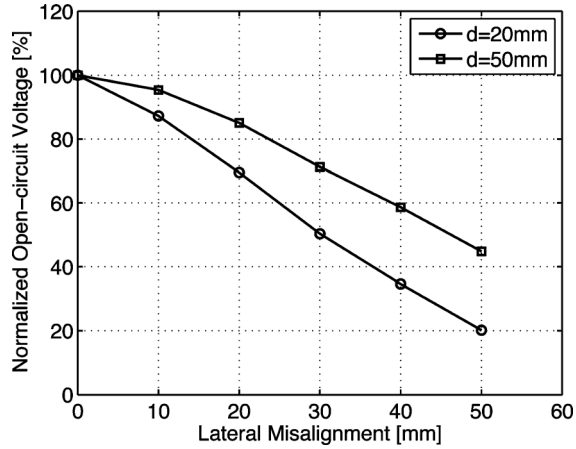

Fig. 12. The normalized induced open-circuit voltage of a 600-turn receiving coil with a diameter of 34 mm at the distance of 20 mm and 50 mm.

B. Misalignement

To demonstrate the versatility of the LF-WPTT, the induced open-circuit voltage of the receiving coil is measured as a function of the lateral misalignment l, which is defined as the lateral distance between the axis of the magnet and the coil, as shown in Fig. 10. When the distance d (labeled in Fig. 10) is 20 and 50 mm, the induced voltage of the receiving coil is measured. The normalized induced voltage is plotted versus l in Fig. 12. When the lateral misalignment reaches 20 mm (i.e., the center of the disk magnet is moved out of the edge of the coil), the induced voltage drops about 30% and 15% at the distance d of 20 mm and 50 mm, respectively.

The induced voltage of the receiving coil is also measured and compared between Configuration A and B, as depicted in Fig. 10, which are the two extreme cases in the angular misalignment. When the coil orientation is changed from Configuration A to B, the induced voltage of the receiving coil is measured in each orientation and recorded in Fig. 13. When the distance d (labeled in Fig. 10) is 20 mm, the induced voltage drops from 14.00 to 7.00 V (corresponding to $\sim 50\%$ reduction), as depicted in Fig. 13. When d is 50 mm, the induced voltage drops from 1.70 to 0.92 V (corresponding to $\sim 46\%$ reduction).

C. Conductive Bio-Tissue

The conductive bio-tissue around the implant greatly complicates the design of the existing RF-WPTT. First, it poses a delicate tradeoff on the operating frequency. A lower operating frequency is generally preferred to avoid absorption loss caused by the conductive bio-tissue [23]. However, a lower operating frequency tends to lower the power delivery efficiency [18], or requires a much larger receiving coil [36]. Second, the conductive bio-tissue will alter the impedance of the receiving coil in RF [22], and consequently, it will impact the overall power delivery efficiency due to the impedance mismatch [22]. Because the conductivity and dielectric constant associated with bio-tissue varies with the different parts of the human body [5], it further complicates the design and implementation of the RF-WPTT.

In the LF-WPTT, the magnetic field produced by the rotating permanent magnets varies at close-to-DC frequencies. Thus, the

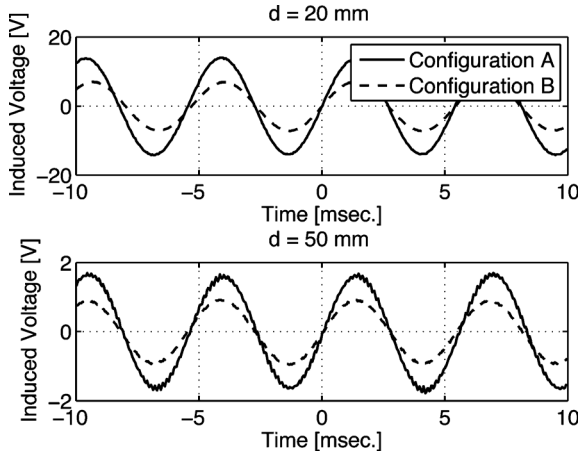

Fig. 13. Induced open-circuit voltages are plotted when the receiving coil is placed in Configuration A and B (with the angular misalignment reaching 90° in latter case). The solid line represents Configuration A, and the dashed line represents Configuration B. The distance between the rotating-magnets and the receiving coil is 20 mm and 50 mm for the upper and lower figure, respectively.

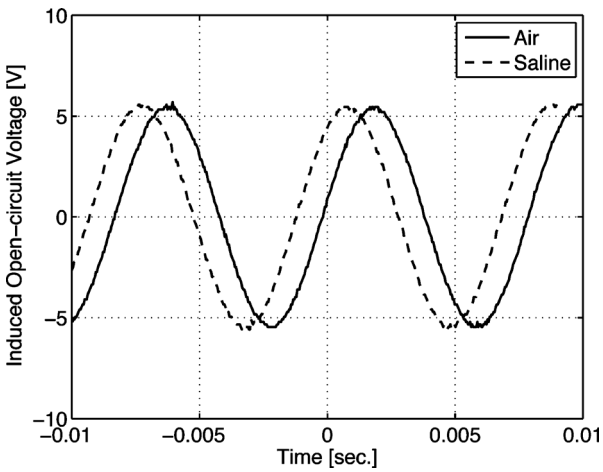

Fig. 14. The induced open-circuit voltage versus time when the receiving coil with 600 turns and 34 mm in diameter is placed in the open air (solid line) and in the saline solution (dashed line).

power loss associated with the conductive bio-tissue is minimized. To demonstrate this experimentally, the induced open-circuit voltage of the receiving coil is measured and compared when it is operated in the open-air or immersed in a saline solution. Because the saline solution's conductivity ($\sigma = 0.6\ \mathrm{S/m}$) is close to that of bio-tissue [37], it is widely used to emulate conductive bio-surroundings [22]. In this experiment, the same receiving coil (with 600 turns and 34 mm in diameter) is placed 20 mm away from the rotating magnets, as defined in Fig. 10, and the distance between the rotating-magnets and the top surface of the saline is 10 mm. The coil is completely immersed in the solution. The measured induced open-circuit voltage in the open-air and in the saline are plotted in Fig. 14 as the solid line and the dashed line, respectively. Fig. 14 demonstrates that there is no noticeable degradation when the receiving coil is immersed in the saline compared to that in the open-air. This experiment shows that the delivered power of the LF-WPTT is unlikely to be impaired by conductive bio-tissues.

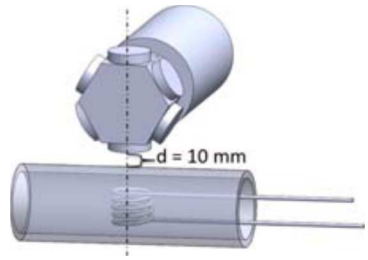

Fig. 15. The receiving coil is housed within a metal tube. The normal axes of the coil and the disk magnet are aligned in a vertical orientation.

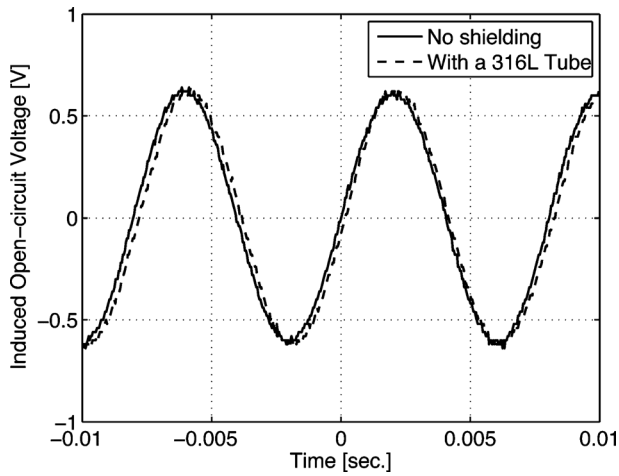

Fig. 16. The induced open-circuit voltage versus time when the receiving coil is in the open air (the solid line) and shielded by a metal tube made of 316L implant-grade stainless steel (the dashed line).

D. Metal Housing

Medical implants, especially orthopedic ones, are often housed in metals for their strength and durability [11]. Due to the low operating frequency, the LF-WPTT has demonstrated negligible losses when the receiving coil is placed inside a cylinder made of the implant-grade stainless steel that is widely used in orthopedic implants. In the experiment, the induced voltage of a receiving coil is measured when it is placed inside a non-magnetic implant-grade stainless steel cylinder, as shown in Fig. 15. In the setup, the metal cylinder is made of 316L, one kind of implant-grade stainless steel with a resistivity of $740\ \mathrm{n\Omega \cdot m}$. The thickness and the outer diameter of the tube are 1.65 mm and 15.90 mm, respectively. The length of the tube is 108 mm. To fit into the tube, the receiving coil is wound into an oval with a long axis of 26 mm and a short axis of 6 mm. The diameter of the wire is 0.25 mm. The receiving coil has 120 turns. The distance d between the rotating-magnets and the metal cylinder (defined in Fig. 15) is 10 mm. The induced voltage is measured when the receiving coil is placed in the center of the cylinder shown as the dotted line in Fig. 16. Compared to the measured induced voltage without the stainless steel cylinder, depicted as the solid line in Fig. 16, there is no noticeable degradation. However, there is about 34% reduction of the induced voltage when the cylinder is made of aluminum with the resistivity close to $28\ \mathrm{n\Omega \cdot m}$. This experiment demonstrates that the receiving coil in the LF-WPTT can be integrated into

an implant in a non-magnetic stainless steel housing without significant power loss.

V. Discussions

In the LF-WPTT, the low operating frequency alleviates some of the constraints that are specific to the high frequency operation in the RF-WPTT. (1) The LF-WPTT avoids the RF radiation, which could be a concern in the high-power transmission [4]. (2) The LF-WPTT simplifies the design of the receiving coil. In the LF-WPTT, the inductance of the receiving coil becomes less of a concern, because ωL is always much less than R_S. Thus, as long as the space permits, the receiving coil prefers to have the maximum number of turns with an optimized ferrimagnetic structure around it for the highest induced voltage. The high induced voltage also favors the subsequent rectifying circuits [38]. (3) The matching between the receiving coil and the load can be optimized without considering a change of the operating environment, because the reactive part of the receiving coil, which is susceptible to the environment, is negligible compared to its resistive part at the low frequency. The resistance of the receiving coil, however, is unlikely to change in different operating environments, e.g., different operating distances or different bio-tissues. Thus, in the LF-WPTT, the efficiency of the power delivery from the receiving coil to the load can always be maintained under various operating environments. (4) Because of the low operating frequencies, switching-based power conditioning circuits, like those used in energy scavenging systems [39], [40], can be used to convert and boost the induced low-voltage AC power to the high-voltage DC power. Compared to traditional rectifying circuits used in the RF-WPTT, the switching-based circuits are more efficient when the induced voltage of the receiving coil is comparable or less than the rectifier's turn-on voltage [41]. (5) The strong and slow changing magnetic field produced by the rotating magnets is able to deliver power wirelessly through non-magnetic materials, including saline (to emulate conductive bio-tissues) and/or stainless steel metal housing, with negligible power loss. (6) Due to the spatial variation of the magnetic field produced by the rotating magnets, the requirements of the geometrical alignment between the *ex-vivo* power source and the *in-vivo* receiving coil can be modestly relaxed.

There are also disadvantages associated with this mechanical-electrical wireless power transfer system. Although the *ex-vivo* rotary system can be shrunk into a torch-light like system for mobile applications [24], it is probably still too bulky for wearable applications. Also, the wireless data communication system needs to be added independently, whereas the RF-WPTT is able to support wireless power transfer and the wireless communication at the same time [42]. However, since the frequencies for the wireless data communication and the LF-WPTT are far apart, low interferences between these two functions are expected.

VI. Conclusion

A novel LF-WPTT is herein presented that uses a rotating magnetic element to wirelessly deliver electrical power to an inductive coil. Utilizing the superior magnetic strength of rare-earth magnets, the new method is able to deliver power at a much lower frequency (< 1 kHz) than the existing RF-WPTT that often operates at MHz to GHz frequencies. The low frequency operation completely avoids the RF radiation hazard and dramatically simplifies the design of the receiving coil and the subsequent power conditioning circuit for high efficient wireless power transfer. Also, the LF-WPTT demonstrates that there is negligible power loss caused by the conductive surroundings when the receiving coil is put into a non-magnetic implant-grade stainless steel housing or immersed in conductive saline solution. The characterization results of this novel LF-WPTT suggest that it is suitable for the near-field wireless power transfer to biomedical implants.

Acknowledgment

The authors would like to thank Mr. G. Kielian for the SolidWorks drawings, as well as Mr. P. Frances and Mr. T. Franco for their machining support. They are all affiliated with San Francisco State University.

References

[1] R. Bashirullah, "Wireless implants," *IEEE Microw. Mag.*, vol. 11, pp. S14–S23, Dec. 2010.

[2] W. H. Ko, S. P. Liang, and C. D. F. Fung, "Design of radio-frequency powered coils for design of radio-frequency powered coils for implant instruments," *Med Biol. Eng. Comput.*, pp. 634–640, Nov. 1977.

[3] A. Kurs, A. Karalis, R. Moffatt, J. D. Joannopoulos, P. Fisher, and M. Soljacic, "Wireless power transfer via strongly coupled magnetic resonances," *Science*, vol. 317, no. 5834, pp. 83–86, Jul. 2007.

[4] U.S. Department of Labor, Occupational Safety & Health Administration [Online]. Available: http://www.osha.gov/SLTC/radiofrequencyradiation

[5] A. Christ, A. Klingenbock, T. Samaras, C. Goiceanu, and N. Kuster, "The dependence of electromagnetic far-field absorption on body tissue composition in the frequency range from 300 MHz to 6 GHz," *IEEE Trans. Microw. Theory Tech.*, vol. 54, no. 5, pp. 2188–2195, Mar. 2006.

[6] N. D. N. Donaldson and T. A. Perkins, "Analysis of resonant coupled coils in the design of radio frequency transcutaneous links," *Med. Biol. Eng. Comput.*, vol. 21, no. 5, pp. 612–627, Sep. 1983.

[7] L. S. Y. Wong, S. Hossain, J. E. A. Ta, D. H. Rivas, and H. Naas, "A very low-power CMOS mixed-signal IC for implantable pacemaker applications," *IEEE J. Solid-State Circuits*, vol. 39, no. 12, pp. 2446–2456, Dec. 2004.

[8] G. Wang, W. Liu, M. Sivaprakasam, and G. Kendir, "Design and analysis of an adaptive transcutaneous power telemetry for biomedical implants," *IEEE Trans. Circuits Syst. I, Reg. Papers*, vol. 52, no. 10, pp. 2109–2117, Oct. 2005.

[9] R. R. Harrison, P. T. Watkins, R. J. Kier, R. O. Lovejoy, D. J. Black, B. Greger, and F. Solzbacher, "A low-power integrated circuit for a wireless 100-electrode neural recording system," *IEEE J. Solid-State Circuits*, vol. 43, no. 1, pp. 123–133, Jan. 2007.

[10] J. Borenstein, "Medicine by micromachine," *IEEE Spectr.*, vol. 46, no. 11, pp. 36–41, Nov. 2009.

[11] F. Burny, M. Donkerwolcke, F. Moulart, R. Bourgois, R. Puers, K. V. Schuylenbergh, M. Barbosa, O. Paiva, F. Rodes, J. B. Begueret, and P. Lawes, "Concept, design and fabrication of smart orthopedic implants," *Med. Eng. Phys.*, vol. 22, no. 7, pp. 469–479, Sep. 2000.

[12] Medtronic EnRhythm Pacemaker [Online]. Available: http://wwwp.medtronic.com/Newsroom/ImageLibraryDetails.do?itemId=1126642166159&lang=en_US

[13] M. A. Wood and K. A. Ellenbogen, "Cardiac pacemakers from the patient's perspective," *Circulation*, vol. 105, pp. 2136–2138, 2002.

[14] R. K. Jarvik, "System considerations favoring rotary artificial hearts with blood-immersed bearings," *Artif. Organs*, vol. 19, pp. 565–570, 1995.

[15] X. Wang, J. Song, J. Liu, and Z. L. Wang, "Direct-current nanogenerator driven by ultrasonic waves," *Science*, vol. 316, no. 5821, pp. 102–105, Apr. 2007.

[16] Y. Shigeta, T. Yamamoto, K. Fujimori, M. Sanagi, S. Nogi, and T. Tsukagoshi, "Development of ultrasonic wireless power transmission system for implantable electronic devices," in *Proc. Wireless Technology Conf.*, Sep. 2009, pp. 49–52.
[17] N. Chaimanonart, M. A. Suster, and D. J. Young, "Two-channel passive data telemetry with remote RF powering for high-performance wireless and batteryless strain sensing microsystem applications," *IEEE Sensors J.*, vol. 10, no. 8, pp. 1375–1382, Aug. 2010.
[18] A. S. Y. Poon, S. O'Driscoll, and T. H. Meng, "Optimal frequency for wireless power transmission into dispersive tissue," *IEEE Trans. Antennas Propag.*, vol. 58, no. 5, pp. 1739–1750, May 2010.
[19] M. Mark, T. Bjorninen, L. Ukkonen, L. Sydanheimo, and J. M. Rabaey, "SAR reduction and link optimization for mm-size remotely powered wireless implants using segmented loop antennas," in *Proc. IEEE Topical Conf. Biomedical Wireless Technologies, Networks, and Sensing Systems*, Phoenix, AZ, Jan. 2011, pp. 7–10.
[20] Y. T. Liao, H. Yao, A. Lingley, B. Parviz, and B. Otis, "A 3-uw CMOS glucose sensor for wireless contact-lens tear glucose monitoring," *IEEE J. Solid-State Circuits*, vol. 47, no. 1, pp. 335–344, Jan. 2012.
[21] F. C. Flack, E. D. James, and D. M. Schlapp, "Mutual inductance of air-cored coils- effect on design of radio-frequency coupled implants," in *Med. Biol. Eng. Comput.*, Jan. 1971, pp. 79–85.
[22] U. M. Jow and M. Ghovanloo, "Modeling and optimization of printed spiral coils in air, saline, and muscle tissue environments," *IEEE Trans. Biomed. Circuits Syst.*, vol. 3, no. 5, pp. 339–347, Oct. 2009.
[23] J. C. Lin, A. W. Guy, and C. C. Johnson, "Power deposition in a spherical model of man exposed to 1–20 mhz electromagnetic fields," *IEEE Trans. Microw. Theory Tech.*, vol. 21, no. 12, pp. 791–797, Dec. 1973.
[24] J. Liu, M. Etemadi, J. Heller, D. Kwiat, R. Fechter, M. Harrison, and S. Roy, "ROBOImplant II: Development of a non-invasive controller/actuator for wireless correction of orthopedic structural deformities," *J. Med. Devices*, vol. 6, no. 3, p. 031006, Sep. 2012.
[25] H. Jiang, J. Zhang, S. Liou, R. Fechter, S. Hirose, M. Harrison, and S. Roy, "A high-power versatile wireless power transfer for biomedical implants," in *Proc. Annu. Int. Conf. IEEE Engineering in Medicine and Biology Soc.*, Aug. 2010, pp. 6437–6440.
[26] P. T. Theilmann and P. M. Asbeck, "An analytical model for inductively coupled implantable biomedical devices with ferrite rods," *IEEE Trans. Biomed. Circuits Syst.*, vol. 3, no. 1, pp. 43–52, Feb. 2009.
[27] Supermagnetman [Online]. Available: http://www.supermagnetman.net
[28] *COMSOL Multiphysics User's Guide*, COMSOL Inc., Los Angeles, CA, 2007.
[29] Faulhaber Group [Online]. Available: http://www.faulhaber.com
[30] Ferroxcube [Online]. Available: http://www.newark.com/ferroxcube/rod5-20-4b1/ferrite-rod-20x5mm/dp/63R5828
[31] U. M. Jow and M. Ghovanloo, "Design and optimization of printed spiral coils for efficient transcutaneous inductive power transmission," *IEEE Trans. Biomed. Circuits Syst.*, vol. 1, no. 3, pp. 193–202, Sep. 2007.
[32] M. Theodoridis and S. Mollov, "Distant energy transfer for artificial human implants," *IEEE Trans. Biomed. Eng.*, vol. 52, no. 11, pp. 1931–1938, Nov. 2005.
[33] M. Kiani, U. M. Jow, and M. Ghovanloo, "Design and optimization of a 3-coil inductive link for efficient wireless power transmission," *IEEE Trans. Biomed. Circuits Syst.*, vol. 5, no. 6, pp. 579–591, Dec. 2011.
[34] C. Zierhofer and E. Hochmair, "High-efficiency coupling-insensitive transcutaneous power and data transmission via an inductive link," *IEEE Trans. Biomed. Eng.*, vol. 37, no. 7, pp. 716–722, Jul. 1990.
[35] J. D. Irwin, *Basic Engineering Circuit Analysis*, 7th ed. New York: Wiley, 2002.
[36] F. Zhang, S. A. Hackwoth, X. Liu, C. Li, and M. Sun, "Wireless power delivery for wearable sensors and implants in body sensor networks," in *Proc. Annu. Int. Conf. IEEE Engineering in Medicine and Biology Society*, Aug. 2010, pp. 692–695.
[37] S. Gabriel, R. W. Lau, and C. Gabriel, "The dielectric properties of biological tissues: II. Measurements in the frequency range 10 hz to 20 ghz," *Phys. Med. Biol.*, vol. 41, no. 11, pp. 2251–2251, Nov. 1996.
[38] H. M. Lee and M. Ghovanloo, "An integrated power-efficient active rectifier with offset-controlled high speed comparators for inductively powered applications," *IEEE Trans. Biomed. Circuits Syst.*, vol. 58, no. 8, pp. 1749–1760, Aug. 2011.
[39] R. Dayal, S. Dwari, and L. Parsa, "Design and implementation of a direct AC-DC boost converter for low-voltage energy harvesting," *IEEE. Trans. Ind. Electron.*, vol. 58, no. 6, pp. 2387–2396, Jun. 2011.
[40] Y. K. Ramadass and A. P. Chandrakasan, "An efficient piezoelectric energy harvesting interface circuit using a bias-flip rectifier and shared inductor," *IEEE J. Solid-State Circuits*, vol. 45, no. 1, pp. 189–204, Jan. 2010.
[41] H. Jiang, D. Lan, D. Lin, J. Zhang, S. S. Liou, H. Shahnasser, M. Shen, M. Harrison, and S. Roy, "A feed-forward controlled ac-dc boost converter for biomedical implants," in *Proc. Annu. Int. Conf. IEEE Engineering in Medicine and Biology Soc.*, San Diego, CA, Aug. 2012, pp. 1675–1678.
[42] S. Mandal and R. Sarpeshkar, "Power-efficient impedance-modulation wireless data links for biomedical implants," *IEEE Trans. Biomed. Circuits Syst.*, vol. 2, no. 4, pp. 301–315, Dec. 2008.

Hao Jiang (M'95) received the B.S. degree in materials sciences and engineering from Tsinghua University, Beijing, China, and the Ph.D. degree in electrical engineering from University of California, San Diego, in 1994 and 2000, respectively.

He has been with San Francisco State University (SFSU) since August 2007 as an Assistant Professor in electrical engineering. Prior to joining SFSU, he worked for the Broadcom Corporation, Jazz Semiconductor, and Conexant Systems Inc. His research interests are in the general area of analog integrated circuits, particularly in ultra-low-power circuits for biomedical applications.

Junmin Zhang received the B.S. and M.S. degrees in electrical engineering from San Francisco State University (SFSU), San Francisco, CA, in 2008 and 2011, respectively.

Since 2011, he has been an Engineer in the School of Engineering at SFSU. From 2008 to 2011, he worked on the low-frequency wireless power transfer technology for biomedical implant in the SF Bioelectronics Lab at SFSU.

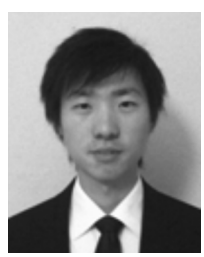

Di Lan (S'09) received the B.S. and M.S. degrees in electrical engineering from San Francisco State University, San Francisco, CA, in 2009 and 2012, respectively.

From 2008 to 2012, he worked on the low-frequency wireless power transfer technology and its power conditioning circuits for biomedical applications. Currently, he is a doctoral student at the University of South Florida, Tampa, working on RF MEMS.

Kelvin K. Chao is a senior student at Mill High School, Millbrae, CA. He was a Research Intern in the Bioelectronics Lab at San Francisco State University, San Francisco, CA, in the summers of 2011 and 2012.

Shyshenq Liou (M'89) received the M.S.E.E. degree and Ph.D. degree in electrical engineering from the University of Texas at Austin in 1985 and 1989, respectively.

In 1991, he joined the School of Engineering, San Francisco State University (SFSU), San Francisco, CA, as an Assistant Professor. In 2006–2007, he was a Senior Visiting Scholar at Tsinghua University, Beijing, China, doing energy efficiency research. He retired from SFSU in August 2012 and now works as a Consultant in building solar projects in the USA and Taiwan.

Hamid Shahnasser (M'89) received the B.S., M.S. and Ph.D. degrees from McGill University, Montreal, QC, Canada, Carnegie Mellon University, Pittsburgh, PA, and Drexel University, Philadelphia, PA, respectively.

His research interests are in the area of computer systems and communication networks and their applications in various domains. His research work has been funded by NSF, NSA and the NASA Ames Research Center and Department of Education, as well as local industries. His work has been presented at many international forums and published in journals and conference proceedings.

Richard Fechter received the B.S degree from the University of Utah, Salt Lake City, in 1979.

He works at the University of California, San Francisco (UCSF), Medical Center and Children's Hospital. He is a Principal Developmental Engineer in the Clinical Engineering Department, and has expertise as an Electrical Engineer, Mechanical Engineer, and Medical Device Incident Investigator. He also works with the UCSF Pediatric Device Consortium and has contributed to numerous peer-reviewed articles and medical device patents.

Shinjiro Hirose received the B.S. degree in mechanical engineering from the Massachusetts Institute of Technology, Cambridge, and received a medical degree from New York Medical College, Valhalla.

He completed three years of surgery training at the University of California, Davis, Medical Center. He completed a general surgery residency and a postdoctoral fellowship at the Fetal Treatment Center Laboratory at the University of California, San Francisco (UCSF), where he researched neural regeneration after spinal cord injury and its implications in fetal surgery for myelomeningocele, a type of spina bifida. He completed a pediatric surgery fellowship at Morgan Stanley Children's Hospital at Columbia University, New York. His research interests include fetal surgery for disorders of twin gestations, congenital diaphragmatic hernia, and gastroschisis. He is an Assistant Professor of Surgery at UCSF.

Michael Harrison graduated cum laude from Yale University, New Haven, CT, and magna cum laude from Harvard Medical School, Boston, MA.

He is Professor Emeritus of Surgery, Pediatrics, and Obstetrics, Gynecology and Reproductive Sciences at the University of California, San Francisco (UCSF). He completed his surgical training at Massachusetts General Hospital, Boston, MA, followed by a pediatric surgery fellowship at the Rikshospitalet, Oslo, Norway, and the Children's Hospital of Los Angeles. He is internationally renowned for his expertise and innovation in pediatric and fetal surgery. He was one of the original founders of the International Fetal Medicine and Surgery Society, the Founding Director of the UCSF Fetal Treatment Center, and most recently, the Founding Director of the UCSF Pediatric Device Consortium. He has authored more than 400 peer-reviewed articles and several textbooks, including three editions of *The Unborn Patient: The Art and Science of Fetal Therapy*. He maintains an active research lab focused on medical device innovation, development, and commercialization.

Dr. Harrison is a member of various medical and surgical professional societies and has been recognized by his colleagues for his contributions to the field, and honored with a number of prestigious awards, including the American College of Surgeons Jacobson Innovation Award, as well as membership into the Institute of Medicine. In 2011, he was the recipient of UCSFs inaugural Distinguished Lectureship in Translational Research.

Shuvo Roy (M'90) received the B.S. degree (magna cum laude) with general honors for triple majors in physics, mathematics (special honors), and computer science from Mount Union College, Alliance, OH, in 1992. He received the M.S. degree in electrical engineering and applied physics and the Ph.D. degree in electrical engineering and computer science from Case Western Reserve University, Cleveland, OH, in 1995 and 2001, respectively.

He is currently an Associate Professor in the Department of Bioengineering and Therapeutic Sciences (BTS), a joint department of the Schools of Pharmacy and Medicine at the University of California, San Francisco (UCSF), and Director of the UCSF Biomedical Microdevices Laboratory. He holds the Harry Wm. and Diana V. Hind Distinguished Professorship in Pharmaceutical Sciences II in the UCSF School of Pharmacy. He is a founding member of the UCSF Pediatric Devices Consortium, which has a mission to accelerate the development of innovative devices for children's health, and a faculty affiliate of the California Institute for Quantitative Biosciences (QB3). From 1998 to 2008, he was Co-Director of the BioMEMS Laboratory in the Department of Biomedical Engineering at the Cleveland Clinic, Cleveland, OH, where he worked with basic scientists, practicing clinicians, and biomedical engineers to develop MEMS solutions to high-impact medical challenges. In 2008, he joined UCSF to continue the development of biomedical devices including wireless physiological monitoring systems and bioartificial replacement organs, and participate in the training of professional students in the School of Pharmacy as well as graduate students in the UCSF/UCB Joint Graduate Group in Bioengineering.

Dr. Roy is an Associate Editor of *Biomedical Microdevices* and editorial board member of *Sensors and Materials*. He has contributed to more than 90 technical publications, coauthored three book chapters, has been awarded 16 U.S. patents, and given more than 70 invited presentations. He is the recipient of a Top 40 under 40 award by Crain's Cleveland Business in 1999 and the Clinical Translation Award at the 2nd Annual BioMEMS and Biomedical Nanotechnology World 2001 meeting. In 2003, he was selected as a recipient of the TR100, which features the world's 100 Top Young Innovators as selected by *MIT Technology Review*. In 2004, he was presented with a NASA Group Achievement Award for his work on harsh environment MEMS. In 2005, he was named in Who's Who in Biotechnology by Crain's Cleveland Business. In 2005 and 2007, he was recognized as a Cleveland Clinic Innovator. In 2009, he was nominated for the Biotechnology Industry Organizations Biotech Humanitarian Award, which is given in recognition of an individual who has used biotechnology to unlock its potential to improve the earth.